Research Square

Preprints are preliminary reports that have not undergone peer review.
They should not be considered conclusive, used to inform clinical practice,
or referenced by the media as validated information.

Computational Identification of Quinolinol-Based Estrogen Receptor Alpha (ER-α) Antagonists as Promising Therapeutics for MCF-7 Breast Cancer

Mayank Garhewal Mayank Garhewal
Guru Ghasidas Vishwavidyalaya
Divya Pujari Divya Pujari
LCIT , Near High Cout, Bodri, Bilaspur
Ayush Tiwari Ayush Tiwari
Guru Ghasidas Vishwavidyalaya
Aditya Mishra Aditya Mishra
Guru Ghasidas Vishwavidyalaya
Arin Bhattacharya Arin Bhattacharya
J K College of Pharmacy, Near Gatora Railway Station
Shekhar Verma Shekhar Verma
Guru Ghasidas Vishwavidyalaya
Achal Mishra Achal Mishra
Guru Ghasidas Vishwavidyalaya
Avantika Agrawal Avantika Agrawal
Guru Ghasidas Vishwavidyalaya
Yogesh Vaishnav Yogesh Vaishnav
yogesh446688@gmail.com

Guru Ghasidas Vishwavidyalaya

Research Article

Keywords: Estrogen Receptor Alpha (ER-α), Breast Cancer (MCF-7), Quinolinol Derivatives, Computer-Aided Drug Design (CADD), 3D-QSAR & Pharmacophore Modeling, Molecular Docking, Molecular Dynamics Simulation

Posted Date: June 22nd, 2026

DOI: https://doi.org/10.21203/rs.3.rs-9843735/v1

License: This work is licensed under a Creative Commons Attribution 4.0 International License.
Read Full License

Additional Declarations: No competing interests reported.

Research Article

Computational Identification of Quinolinol-Based Estrogen Receptor Alpha (ER-α) Antagonists as Promising Therapeutics for MCF-7 Breast Cancer

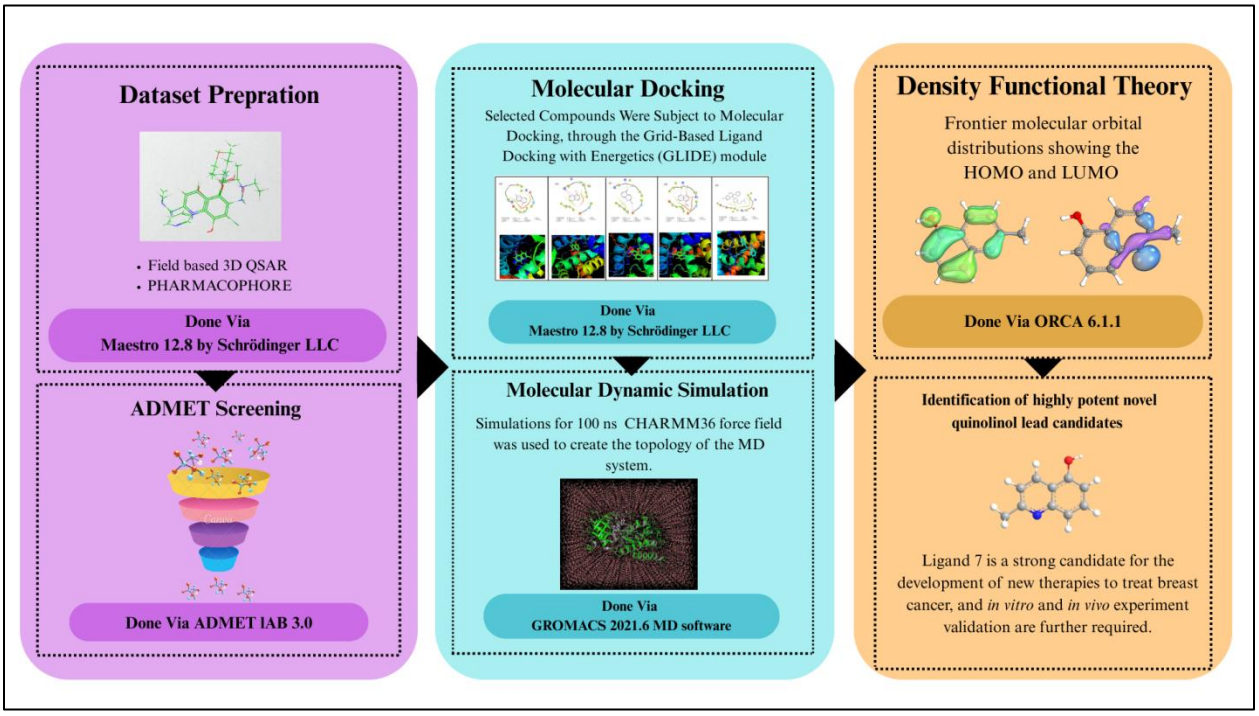
Mayank Garhewal[1], Divya Pujari[2], Ayush Tiwari[1], Aditya Mishra[1], Arin Bhattacharya[3], Shekhar Verma[1], Achal Mishra[1*], Avantika Agrawal[1*] and Yogesh Vaishnav[1,*]

[1]*Department of Pharmacy, Guru Ghasidas Vishwavidyalaya (A Central University), Bilaspur 495009, Chhattisgarh, India;*

[2]*LCIT School Of Pharmacy, Near High Cout, Bodri, Bilaspur, CG, 495220;*

[3]*J K College of Pharmacy, Near Gatora Railway Station, Bilaspur, CG*

Graphical Abstract



***Address correspondence to these authors at** Department of Pharmacy, Guru Ghasidas Vishwavidyalaya (A Central University), Bilaspur, Chhattisgarh-495009, India; E-mail: yogesh446688@gmail.com; Contact: +91 7974495675 (Cell); ORCID ID: 0000-0002-1726-5318.

***Address correspondence to these authors at** Department of Pharmacy, Guru Ghasidas Vishwavidyalaya (A Central University), Bilaspur, Chhattisgarh-495009, India; E-mail: achal.mishra@ggu.ac.in ; Contact: +91 9691054057 (Cell); ORCID ID: 0000-0002-3196-3390.

Abstract

Breast cancer is a major cause of death from cancer worldwide, with the estrogen receptor alpha (ER-α) being an important therapeutic target for hormone-dependent MCF-7 breast cancer. The goal of this study was to use an computer-aided drug design (CADD) methodology to assess 22 quinolinol analogues as potential ER-α antagonists. The CADD methodology consisted of Gaussian field-based three-dimensional quantitative structure-activity relationship (3D-QSAR) analysis, pharmacophore modeling, a prediction of ADMET properties, molecular docking, molecular dynamics simulation (MD), and density functional theory (DFT) calculations. 3D-QSAR model had good predictive ability ($R^2 = 0.9516$, $Q^2 = 0.5989$, RMSE = 0.82, and Pearson's r = 0.845). The results of the pharmacophore analysis showed that the critical features for anticancer activity are an aromatic ring, hydrophobic, and hydrogen bond acceptor. According to the ADMET evaluation, compounds 1, 7, 25, and 13 have the highest potential to be developed into drug-like substances; compound 1 has the best ADMET score of 6.348. The molecular docking study of the ligands with ER-α (PDB ID: 3ERT) demonstrated that ligands 7, 1 and 25 exhibit significantly better binding affinities (-11.98, -11.48, and -11.04 kcal/mol, respectively) than 4-hydroxytamoxifen (-8.26 kcal/mol). The MD simulations showed that ligand 7 formed a considerably more compact and stable ER-α complex through consistent hydrogen bond interactions for the duration of the simulation (100 ns). The DFT analyses indicated ligand 7 had kinetic stability and significantly better electronic properties than the other ligands studied. ligand 7 for the development of breast cancer drugs that target ER-α.

Keywords Estrogen Receptor Alpha (ER-α), Breast Cancer (MCF-7), Quinolinol Derivatives, Computer-Aided Drug Design (CADD), 3D-QSAR & Pharmacophore Modeling, Molecular Docking, Molecular Dynamics Simulation

1 Introduction

Computational methods combined with rationally designed drugs provide a new way to manage the global health care challenge that is hormone sensitive breast cancer. Luminal subtypes of breast cancers A and B account for roughly 70-75% of all breast cancer diagnosis, based on research findings [1]. The luminal subtypes have high levels of expression of estrogen receptor alpha (ER-α) which is a transcription factor that requires binding to the ligand (17β-estradiol) to undergo dimerization within the cytoplasm and move to the nucleus to activate the genomic transcription of genes responsible for cellular proliferation and angiogenesis [2]. Selective Estrogen Receptor Modulators (SERMs) such as Tamoxifen and its active metabolite 4-hydroxytamoxifen (4-OHT) competitory inhibit the binding of ER-α to its ligands (the binding domain of the ligand is called a ligand binding domain (LBD)) as shownn in Fig. **1** [3]. The long-term effects of SERMs on the reduction in mortality has become problematic due to the development of hormone resistance, mainly via genetic mutations in the ESR1 gene or potentially undesirable side effects (e.g., endometrial hyperplasia) resulting from the prolonged exposure to ER-α modulators [4,5]. Therefore, an immediate clinical need exists for the development of structurally diverse, novel ER-α antagonists, with nitrogen containing heterocycles providing a productive area of exploration since they are commonly used to develop FDA approved ER-α antagonists [6]. Among these, quinolinol has become an important structure in medicinal chemistry "privileged scaffold". The ability for the quinolinol structure to orient itself accurately in the hydrophobic region of protein pockets is made possible by its planar, bicyclic heteroaromatic structure. Quinolinol participates in important π–π stacking interactions with aromatic groups (e.g., Phe, Tyr, Trp) and makes hydrogen bonding by its nitrogen and hydroxyl groups, with modifications at the C-3, C-6 and C-8 positions having considerable promise for increasing binding affinity towards the MCF-7 cell line [7].

Traditional drug discovery processes are limited because of their high costs and high attrition rates, but the use of Computer Assisted Drug Design (CADD) offers researchers an accelerated method for modeling biological and metabolic activities in a more condensed time frame [8]. An essential component of a ligand-based method of CADD is the use of Three-Dimensional Quantitative Structure Activity Relationship (3D QSAR) modeling that uses Gaussian Field Analysis (GFA) and Partial Least Squares (PLS) regression analysis to correlate known biological activity (pIC50) with 3D scalar fields such as sterics and electrostatics (contour mapping) [9]. The resulting contour maps provide accurate architectural references for determining optimal placement of substituents to maximize efficacy. In addition to contour mapping, pharmacophore modeling provides additional refinement when choosing candidates for high-throughput screening (HTS) [10]. Using the same principles of physics and computational algorithms, structure-based methods evaluate the binding thermodynamics of a chosen candidate in the active site using techniques such as Grid-Based Ligand Docking with Energetics (GLIDE) [10]. In order to assure a candidate's successful clinical use, *in silico* ADMET prediction provides researchers with information to eliminate candidates with potential liabilities, such as hERG channel inhibition and low oral bioavailability [11]. The 100-nanosecond Molecular Dynamics (MD) simulations using CHARMM36 Advanced Forcefield Mimicking this information will aid in visualising the Conformational evolution of protein-ligand interactions within dynamic cellular environments and will establish the stability and persistence of hydrogen bonds throughout physiological conditions through the calculation of metrics (RMSD, RMSF) associated with their length and distance from each other [12]. The study involves a multi-tier analysis of 22 structurally aligned quinolinol analogue compounds to develop predictive Models for strong antagonism compared to tamoxifen

based on compound-specific substitution patterns. The Integrated use of 3D-QSAR predictive modelling, XP Molecular Docking of the antagonist against the Active Site of the Estrogen Receptor (PDB ID 3ERT) and rigorous MD validation through use of the same methods is to give a sound framework for developing the next generation of anti-breast cancer drugs.

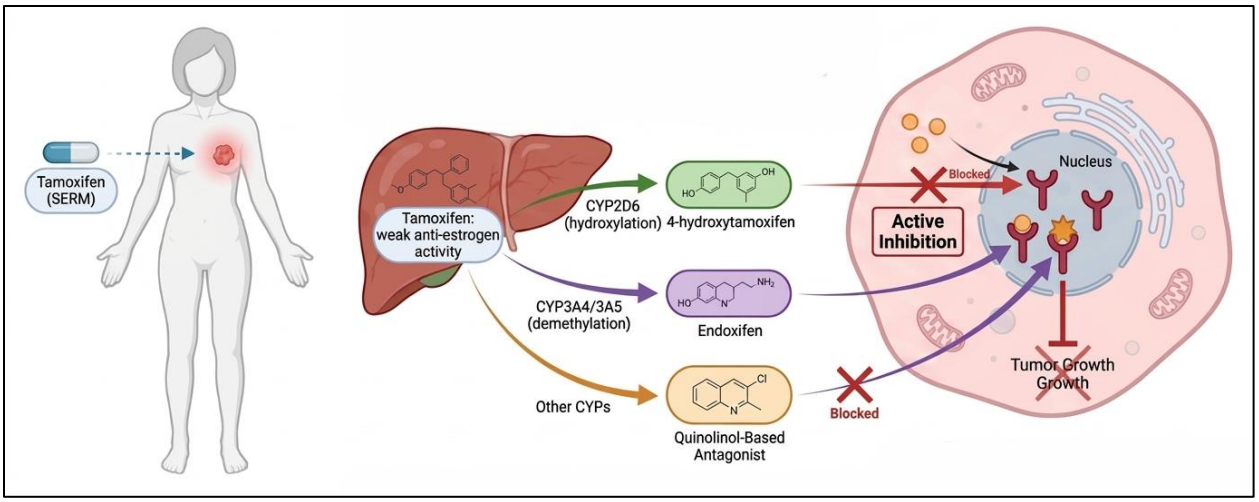


Fig. 1 Quinolinol-Based Antagonist Against Traditional Hepatic Tamoxifen Metabolites.

2 Materials and methods

2.1 Computer and software information

In this study, the processes for producing proteins, preparing ligands, performing field based 3D - QSAR, predicting of ADME properties, and modelling of pharmacophores, were all executed through the use of Maestro 12.8 software produced by Schrödinger LLC., New York (USA). Preparation of virtual screening databases was achieved using PHASE module, whilst the methodology of performing virtual screening studies was accomplished using the methodology of Virtual Screening Workflow (VSW). All molecular modelling and docking studies were performed on a notebook personal computer containing the following specifications: 12th Generation Intel® Core™ i5-1240P Processor @ 1.70 GHz, 8 GB RAM Intel® Iris® Xe Graphics, 64 bit Windows Operating System with x64 Based Architecture. The chemical structures for the ligand library were drawn using ChemDraw Professional 16.0 software.

2.2 Protein Preparation

Protein prep involves both the conversion of 3D macromolecular structures (e.g., proteins) into an appropriate format for conducting molecular docking studies (i.e., docking). The completion of protein preparation is necessary for conducting steps such as bond optimization, adding hydrogen bonds, correcting bond orders, removing atomic clashes and deleting unwanted water from protein crystal structures before docking can be performed. The 3D crystal structure for the human estrogen receptor alpha (ER-α) related to breast cancer was obtained from the protein data bank (PDB ID: 3ERT) (RCSB PDB). The selected protein exhibited satisfactory crystallographic parameters; in this case 1.9 Å resolution, R value of 0.262 and observed R value (R) of 0.229. Protein preparation was performed using the Protein Preparation Wizard in Maestro 12.8 software

(Schrödinger LLC, New York, NY, USA). During preparation, steps taken included correcting bond order/charge, adding hydrogen atoms, optimizing hydrogen bonding networks and deleting water molecules from the crystal structure. Finally, the final protein structure was minimised and optimised using the OPLS4 force field to generate an appropriate stable conformation of the protein structure for use in molecular docking [13].

2.3 Ligand Preparation

The ligand library utilized in 3D-QSAR analysis was created from thirty-two anticancer compounds with significant anti-cancer activity against the MCF-7 breast cancer cell line sourced from the PubChem database. The biological activity data were generated from the MTT assay procedures and IC_{50}s reported in micromolar concentrations (μM). The range of inhibitory activity reported for the compounds was broad, with IC_{50}s ranging from 2.1 to 45.01 μM. The preparation of ligands was performed utilizing the LigPrep module of Maestro 12.8 software (Schrödinger LLC), in conjunction with the Epik tool. For each ligand, a single low-energy conformer was generated using OPLS4 force field, with subsequent desalting and neutralisation to physiological pH. The IC_{50}s were included in the dataset and converted to pIC_{50} for the purposes of subsequent QSAR analysis [14].

2.4 Field Based 3D QSAR Modeling

To create three-dimensional quantitative structure-activity relationships (3D-QSARs), a ligand library with 22 members was utilized to create a dataset that was split into a random training group (70%) and a random test group (30%) for creating and testing models. For the analysis of structure activity relationships (SARs), an analysis technique was the Partial Least Squares (PLS) method to establish the linear correlation among the five Gaussian field descriptors steric, charge electrostatic, hydrophobic, hydrogen-bond acceptor and hydrogen-bond donor fields. The generated models were assessed through a number of different statistical parameters: regression coefficient (R^2), cross-validated regression coefficient (Q^2), standard deviation (SD), root mean square error (RMSE), Pearson's r value, and cross-validation coefficient (R^2CV). From the generated models, the best statistical performance was selected to be the optimal QSAR model. Five different colored contour maps were used to depict the sites that would be favored and disfavored from a spatial standpoint, based on type(s) of chemical interaction(s) and functional group replacement(s), for exhibiting an anticancer effect against the MCF-7 breast cancer cell line [15].

2.5 Pharmacophore Modelling

Pharmacophore modelling was performed using the Phase module integrated in Maestro 12.8 software from Schrödinger LLC. All prepared 22 compounds that showed anticancer activity against the MCF-7 breast cancer cell line were loaded into the “Develop Pharmacophore Hypothesis” panel of the PHASE tool. Six pharmacophoric features were associated with the development of pharmacophore hypotheses: Hydrogen donor (D), Hydrogen acceptor (A),

Aromatic ring (R), Hydrophobic group (H), Positive charge (P), and Negative charge (N). Generated pharmacophore models were compared and scored based on three categories: survival, fitness and molecular alignment to the identified pharmacophoric structures. Best pharmacophore hypothesis was determined by designating compounds with $pIC_{50} \geq 6.5$ as active and compounds with $pIC_{50} \leq 4.5$ as inactive [16].

2.6 ADMET Calculation

The ADMETlab 3.0 web server was used to evaluate the pharmacokinetic and toxicity of the quinolinol derivatives. The analysis was done *in silico* via the run of canonical SMILES through the ADMETlab 3.0 program conducted for in silico prediction of absorption, distribution metabolism, excretion, and toxicity (ADMET) profiles. The ADMET profiles are the physicochemical and pharmacokinetic parameters, specifically with respect to the following:

(i) Molecular Weight
(ii) Number of hydrogen bond donors and acceptors
(iii) Lipophilicity (LogP)
(iv) Aqueous Solubility
(v) Human Intestinal Absorption
(vi) Caco-2 Permeability
(vii) Oral Bioavailability
(vii) Blood-Brain Barrier Permeability
(viii) Plasma Protein Binding
(ix) P-glycoprotein interaction

On top of the previous 9 points, analysis of the metabolic properties was also conducted against inhibition and substrate specificity of cytochrome P450 enzymes, intended to evaluate metabolic stability. In addition, predicted hepatotoxicity, carcinogenicity, mutagenicity, hERG inhibition, and acute oral toxicity were also included in the evaluation of toxicity to the compounds tested [17].

2.7 Molecular Docking

Using Maestro 12.8 software (from Schrödinger LLC) for molecular docking of all the virtually screened compounds, docking energy (in kcal/mol) was estimated, through the Grid-Based Ligand Docking with Energetics (GLIDE) module, from the protein-ligand binding interaction and also managed ligand flexibility during the docking process. Study was done using both Standard Precision (SP) and Extra Precision (XP) docking protocols to screen ligands by obtaining reliable binding conformations and docking scores. After docking completed, analysis of important intermolecular interactions such as hydrogen bonds, hydrophobic and π-π stacking in the active site of the target protein was performed for the screened ligands. In addition, potential molecules with activity against the MCF-7 breast cancer cell line were determined based upon the interaction profile, docking score and binding orientation.

2.8 Molecular Dynamic Simulation

We have carried out molecular dynamics (MD) simulations for 100 ns to investigate the protein-ligand binding interactions and stability of ligand 7 and 4-OHT, the most potent inhibitory substances. The simulations were performed using GROMACS 2021.6 MD software. CHARMM36 force field was used to create the topology of the MD system, with TIP3P water model used to create all of the water in the system. Each of the two systems of protein-ligand complex was solvated using a cubic box of water, in which there was 1.5 nm away from each of the four walls. Sufficient amount of counter ions (i.e. Na+ and Cl-) have been added to the MD box of water to create neutrality in the complete MD system.

The prepared systems were subjected to energy minimization using the steepest descent method to remove steric clashes and unfavorable contacts. Following energy minimization, the systems were equilibrated in the NVT ensemble for 500 ps at a temperature of 310 K, using a coupling constant of 0.1 ps with the Nose–Hoover thermostat, and then equilibrated in the NPT ensemble for 500 ps at a pressure of 1 bar using the Parrinello–Rahman barostat. The equilibrated systems then underwent a production MD simulation run lasting for 100 nanoseconds (ns) using a time step of 2 fs. The bond lengths were constrained using the LINCS algorithm. Long-range electrostatic interactions were treated using the Particle Mesh Ewald (PME) method with a grid spacing of 0.16 nanometers (nm). A cut-off radius of 1.2 nm was applied for long-range electrostatic interactions, and a cut-off distance of 1.0 nm was applied for van der Waals interactions, during the simulation. After completing the MD trajectories of the systems, the MD trajectories were analyzed with GROMACS analysis tools for the determination of key structural stability parameters (i.e., RMSD, RMSF, and Rg) in order to evaluate the dynamic stability and compactness of the protein–ligand complexes [18].

2.9 Density Functional Theory Calculation of Ligand 07 and O-HT

Density functional theory calculations using the Becke 3-parameter, Lee-Yang-Parr (B3LYP) hybrid exchange-correlation (XC) functional with 6-311G+(d,p) basis set were performed for ligand 7 and 4-OHT. The only calculations that were to perform full geometry optimizations and vibrational frequency analyses at the B3LYP/6-311G+(d,p) level of theory on optimized molecular structures. The vibrational analysis of the optimized structures showed no imaginary frequencies and therefore validated that the geometry of the molecules correspond to true local minima along their potential energy surfaces [19]. All of these calculations utilized the default convergence criteria within the Avogadro-ORCA software package. The distribution of HOMO and LUMO for Ligand 07 and 4-OHT were visualized using the IBOView program.

3 Results and discussion

3.1 Field based 3d qsar modeling

The anticancer activity of 22 coumarin derivatives was evaluated against the MCF-7 breast cancer cell line using the Gaussian field-based 3D-QSAR method. This method builds upon the established models CoMFA and CoMSIA to predict biological activity based on molecular and steric structure (Fig. **2**).

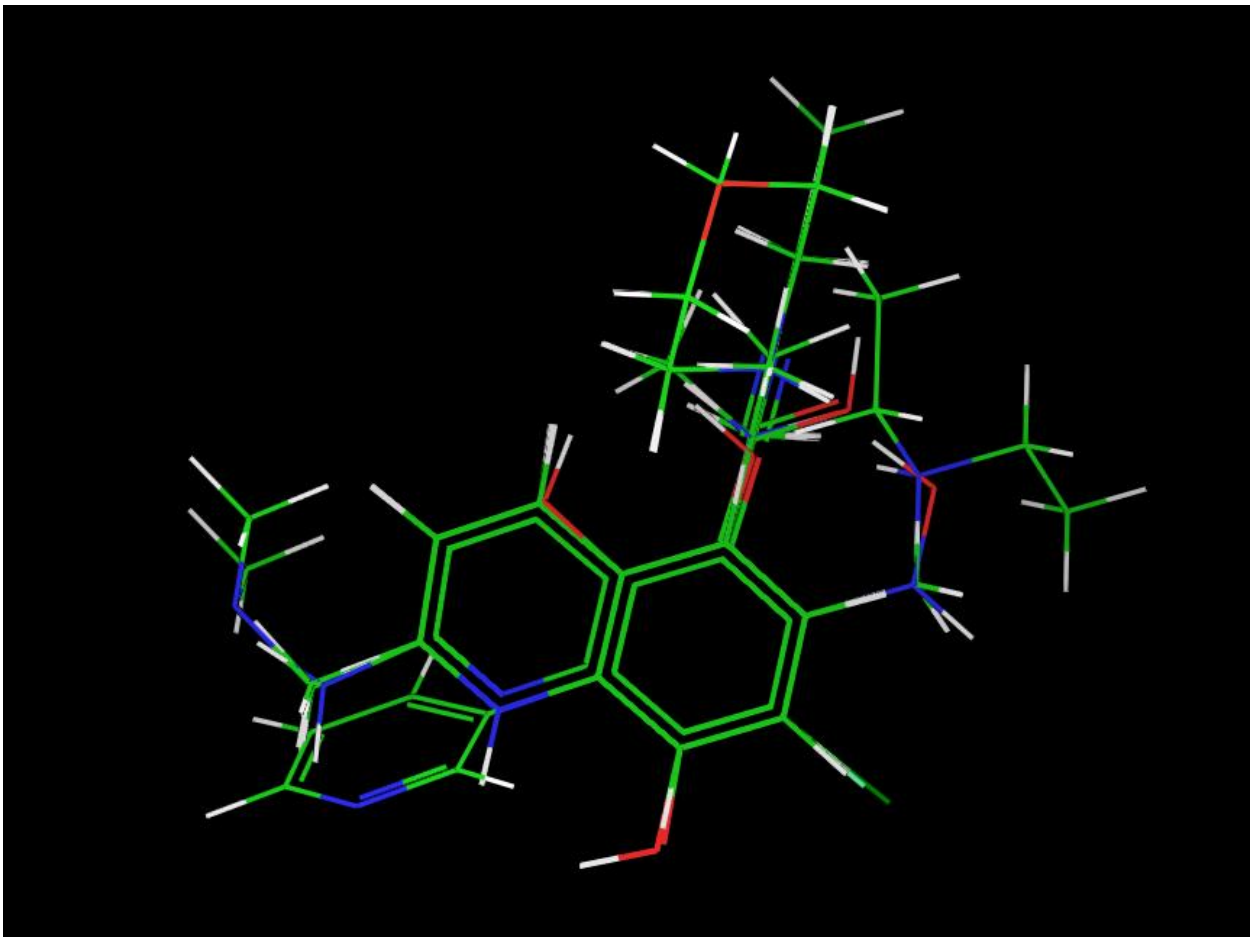


Fig. 2 Aligned 22 compounds of quinolinol derivatives for QSAR modelling.

The 3D-QSAR model for predicting pIC_{50} values (the logarithm of the amount required to inhibit an enzyme or cell line by 50%) used Partial Least Squares (PLS) to analyze the data. After conducting PLS regression on the dataset, the optimal model at PLS factor 3 yielded the highest statistical significance with an SD of 0.2699, an R^2 of 0.9516, a Q^2 of 0.5989, an R^2CV of 0.1933, an R^2 scramble score of 0.8107, a stability score of 0.249, an F value of 102.9, a P value of 6.78×10^{-18}, an RMSE of 0.82, and a Pearson's r of 0.845. In constructing the model, the dependent variable was defined as the pIC_{50} value of each compound, while five Gaussian field descriptors (steric, electrostatic, hydrophobic, hydrogen bond acceptor, and hydrogen bond donor fields) were used as independent variables (Table **1**).

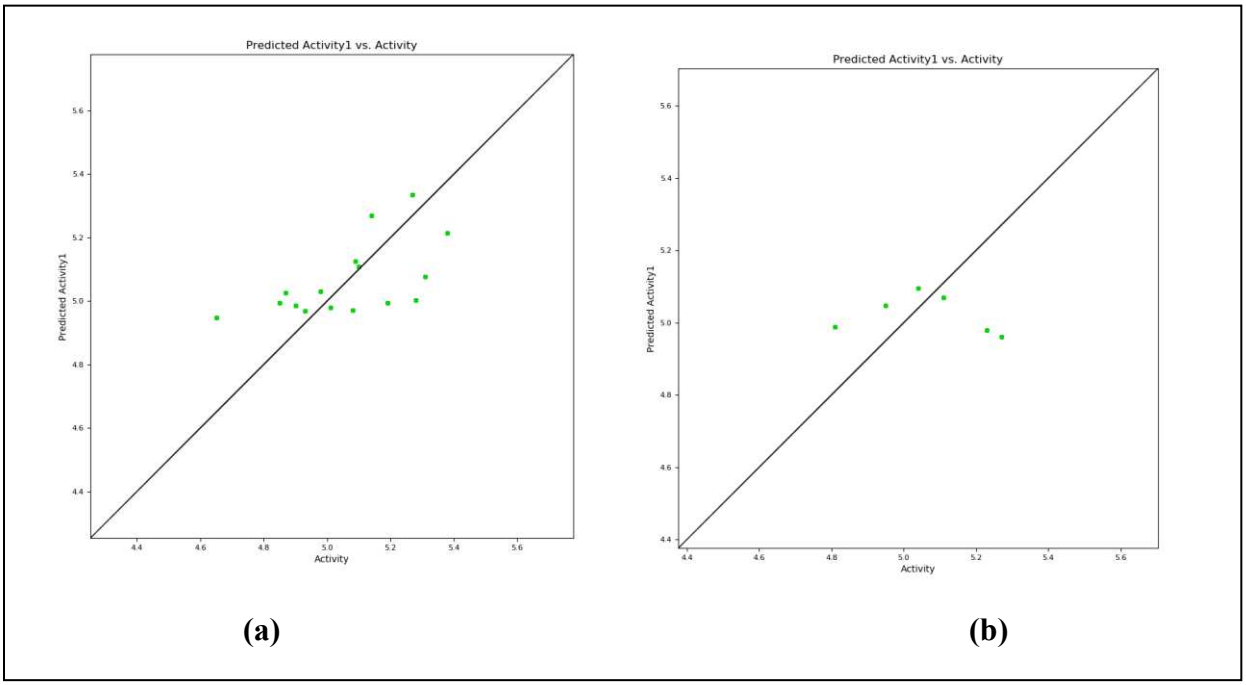
Table 1. Field-based 3D-QSAR modelling parameters.

PLS Factors	SD	R^2	R^2CV	R^2 Scramble	Stability	F Value	P Value	RMSE	Q^2	Pearson-r
1	0.3711	0.8873	0.1417	0.728	0.319	48.9	1.69 ×	0.74	0.6847	0.8139

							10^{-13}			
2	0.3697	0.9298	0.1289	0.739	0.270	63.9	6.99×10^{-15}	0.83	0.6701	0.9124
3	0.2699	0.9516	0.1933	0.8107	0.249	102.9	6.78×10^{-18}	0.82	0.5989	0.845

At PLS factor 3, both the R-squared values and the RMSE values were low, indicating a minimal prediction error and a high degree of robustness of the produced model. The R-squared value was close to 1, suggesting an excellent correlation between the observed and predicted activities of the training set in the laboratory, while Q-squared demonstrated an acceptable degree of predictive ability for the external testing set. The combination of both a low probability value "P" and a high "F" value demonstrated that the statistical reliability and predictive strength of the QSAR model that was developed were substantiated. The external validation of the model was supported by the Pearson's r value of 0.845, which indicates a strong positive linear relationship between the observed and predicted biological activity for each compound in the testing set.

To further confirm the predictive ability of the selected 3D-QSAR model, scatter plots were produced representing the predicted verses experimentally determined (in the laboratory) pIC_{50} values for the entire training and testing sets. The scatter plots demonstrated that the majority of the compounds in both the training and testing sets were clustered closely about the linear regression line, which confirms the robustness, accuracy, and predictive ability of the Gaussian field based 3D-QSAR model developed (Fig. **3**).



(a) **(b)**

Fig. 3 Scatter plot of experimental activity vs predicted activity at PLS factor 3 of **a** Training set of quinolinol derivatives. **b** Test set of quinolinol derivatives.

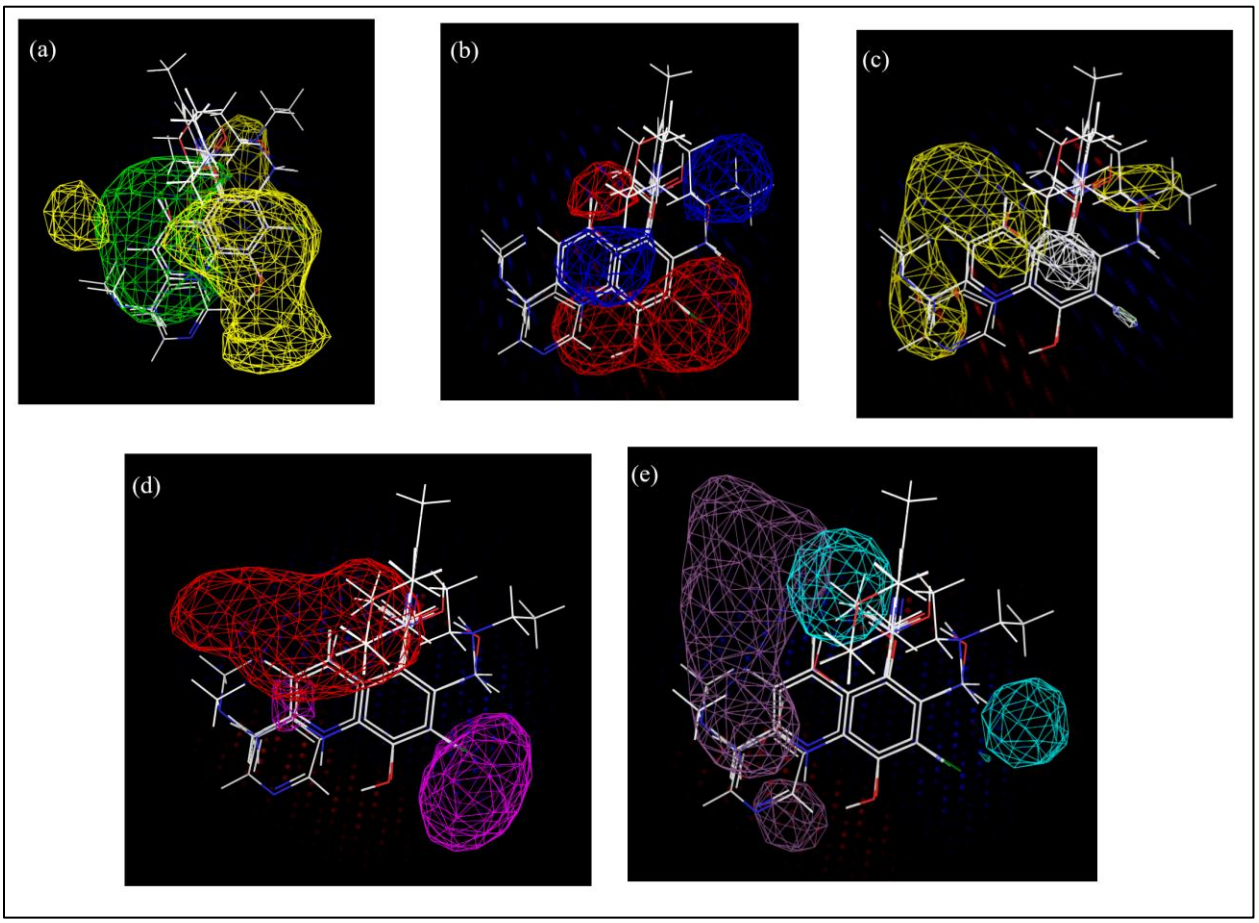


Fig. 4 Contour maps of gaussian of **a** Steric, **b** Electrostatic, **c** Hydrophobic, **d** H-bond acceptor and **e** H-bond donor.

The 3D-QSAR contour maps, based on the Gaussian fields and derived from a set of 22 aligned quinolinol derivatives, revealed several important characteristics that are necessary for effective anticancer activity against the MCF-7 breast cancer cell line. Fig. **4** contains representations of the contour maps for the quinolinol derivatives, including a significant amount of contribution to the total contour maps from steric (36.36%), electrostatic (9.85%), hydrophobic (21.7%), hydrogen bond acceptor (21.13%), and hydrogen bond donor (10.64%) fields; this information provides evidence of the location of favourable and unfavourable sites that impact biological activity. Each of the different colours that appeared on the contour maps indicates the

different physicochemical characteristics required to improve activity against breast cancer cells. Figs. **4**a-e illustrate the contributions from these fields to the total contour maps.

In the 3D-QSAR steric contour map (Fig. **4**a), the green colour's corresponding contour regions indicate that the incorporation of bulky substituents at positions C-3, C-6, and C-8 of the quinolinol scaffolds are advantageous in terms of anticancer activity; conversely, the yellow contour regions indicate where bulky substituents are less than optimal for effective anticancer activity. Thus, introducing bulky aromatic or hydrophobic substituents at C-3, C-6, or C-8 will likely enhance the anticancer activity of quinolinol scaffolds against the MCF-7 cell line. The electrostatic contour map (Fig. **4**b) showed blue and red contour areas corresponding to positive and negative electronic substituents (electropositive and electronegative), respectively. The blue areas near the C-4, C-5, C-6, and C-7 areas indicate that the electron-donating or electropositive groups in these areas will increase the anticancer activity (directly or additively). In contrast, the red regions along the outer edges of the C-3, C-6, and C-8 areas indicate that the electron-withdrawing or electronegative groups in these areas are preferred to provide improved binding interactions with the biological target related to progression of breast cancer. The hydrophobic contour map (Fig. **4**c) showed favorable hydrophobic regions (yellow) near the C-3, C-6, and C-8 areas (outside of the quinolinol ring system), indicating that adding hydrophobic substituents to these areas would increase the MCF-7 inhibition profile. Absence of favorable hydrophobic areas near the C-7 position indicates that adding hydrophobic substituents to this area may decrease biological potency. The hydrogen bond acceptor contour map (Fig. **4**d) indicated that there were favorable (magenta) regions near oxygen containing functionalities of quinolinol derivatives, reflecting the need for hydrogen bond acceptor groups for appropriate binding to the receptor. Favorable acceptor groups near the C-2 and adjacent areas also were shown to be beneficial for increasing anticancer activity. The topography of the hydrophobic contour (Fig. **4**c), portrayed in orange (for hydrophobic) and red (for hydrophilic) regions, points to how ligand binding would be influenced by hydrophobic or hydrophilic acceptor groups located around the ligand of interest. Likewise, the contour distribution of the hydrogen bond donor field (Fig. **4**e) revealed that favorable regions (cyan) were present on the periphery of certain areas of the quinolinol scaffold; hydrogen bond donor groups within these regions would enhance molecular interactions with the active site residues of the target protein in MCF-7 breast carcinoma cells. The overall distribution of contour maps communicates that for the anticancer potential of quinolinol derivatives, there is optimised balance of steric volume, physical characteristics of the compound, the degree of hydrophobicity, and the capability for hydrogen bonding.

The use of Gaussian field-based three-dimensional contour analysis has provided an in-depth understanding of the required molecular modifications necessary to enhance the activity of quinolinol derivatives against the MCF-7 breast carcinoma cell line; therefore, Gaussian field-based contour analysis has the potential to serve as the basis for the rational development of novel breast cancer therapeutics.

3.2 Pharmacophore Modeling

Regarding the pharmacophore modelling investigation, a solid and statistically significant pharmacophore hypothesis was produced regarding quinolinol derivatives displaying anticancer activity toward the MCF-7 breast cancer cell line. Using the pharmacophore model produced, the essential three-dimensional arrangement of chemical features necessary for effective biological activity and ligand-target interaction were determined (Fig. **5**).

As seen in Fig. **5**a, the three-dimensional arrangement of the pharmacophoric features is defined. The pharmacophore hypothesis produced utilised mostly aromatic ring features (R), hydrogen bond acceptor features (A), and hydrophobic regions (P) around the quinolinol scaffold. The aromatic ring features (shown as orange ring contours) confirmed the role of aromatic π-electron interactions stabilising the binding of ligands within the active site of the receptor. The hydrogen bond acceptor features (shown as pink spheres, with directional vectors) indicated that there are electron-rich heteroatoms that accept hydrogen bonds and that these types of atoms play a critical role in increasing anticancer activity against the MCF-7 line. Grey spheres that are shown overlapping the pharmacophoric points denote the range of permissible spatial tolerance areas that are needed for proper ligand alignment and receptor interaction. The alignment of reference compounds displaying the greatest activity against MCF-7 is seen in Fig. **5**b compared to the proposed pharmacophore hypothesis. The "active" quinolinol derivative contained all of the necessary pharmacophoric features in alignment with the structural arrangement of the compound relative to its biological activity, thereby demonstrating a strong relationship between the two. The aromatic components of the reference molecule were well-aligned with the aromatic pharmacophoric features. The oxygen-containing functional groups of the active quinolinol derivatives were also found to match the hydrogen-bond acceptor sites on the pharmacophore very well. These compatible relationships provided assurance of the reproducibility of the artificially created pharmacophore from this study to search for anticancer agents. The alignment of the 22 active quinolinol derivatives to the pharmacophore model is illustrated in Fig. **5**c. Most of the active quinolinol derivatives were found to significantly overlap or exhibit satisfactory correspondence with the pharmacophoric features of the pharmacophore hypothesis, thus supporting that the pharmacophore hypothesis can be used uniformly to identify multiple structurally diverse active molecules. The similarity in the alignment pattern suggests that both the presence of aromatic interactions and the presence of hydrogen-bond acceptor functionalities are important structural characteristics for producing an active compound with inhibitory activity against the MCF-7 breast cancer cell line. The superimposition of the quinolinol derivative molecular structures demonstrates that the pharmacophore model produced in this study is a good predictor of activity and should therefore, if used appropriately, provide a successful means of virtually screening future compounds and designing new quinolinol based potent anticancer agents.

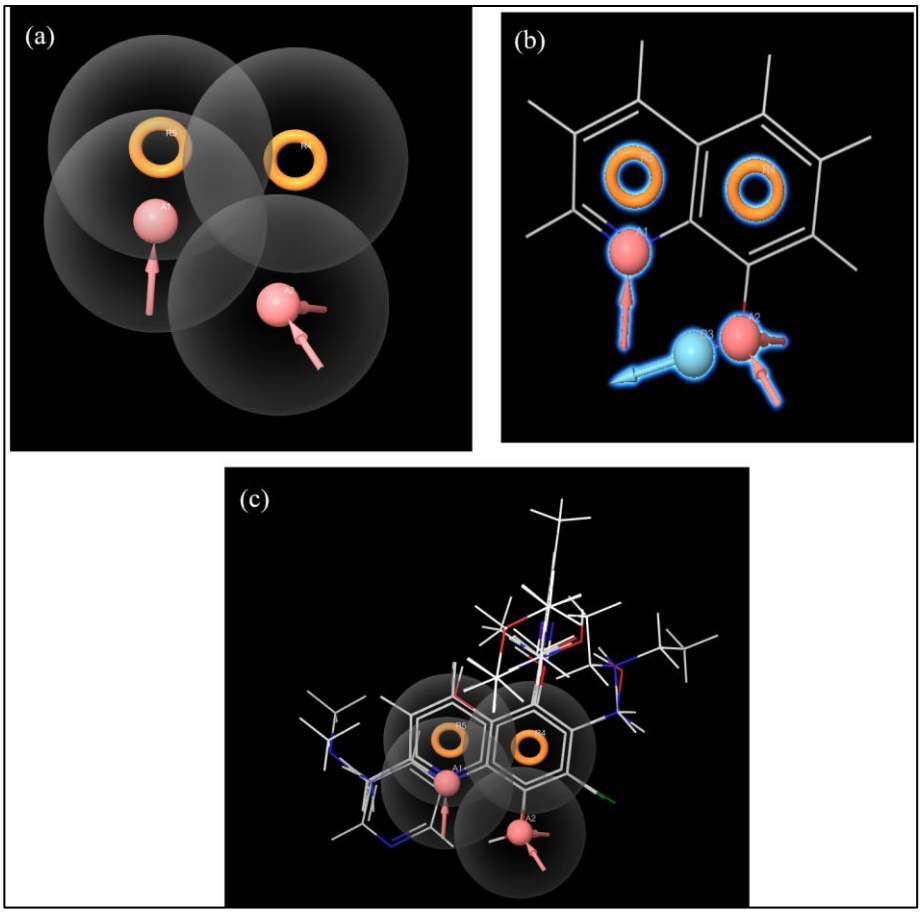


Fig. 5 **a** spatial arrangement of pharmacophoric features. **b** Alignment of reference compound of actives. **c** Alignment 22 compounds of actives.

3.3 ADMET Study

The ADMET assessment of all twenty-two quinolinol derivatives involved examining ten significant pharmacokinetic and toxicity parameters: molecular weight (MW), lipophilicity (logP), aqueous solubility (logS), Caco-2 permeability,human intestinal absorption (HIA), oral bioavailability (F20), blood-brain barrier permeability (BBB), hERG toxicity, DILI toxicity, and Ames mutagenicity prediction. In addition, each compound was ranked by its overall drug-like and pharmacokinetic properties based on the total ADMET score obtained from the combined analysis of the ADMET parameters measured against the MCF-7 breast cancer cell line. The compound with the best ADMET profile and highest score (6.348), is Compound 1 (most favorable), followed by Compound 7 (6.213), Compound 25 (5.768), and Compound 13 (5.706). All four of these compounds demonstrated an adequate combination of favorable physicochemical properties, excellent solubility, acceptable lipophilicity, maximum oral bioavailability, and lower risk of toxicity compared to the other quinolinol derivatives. In particular, Compound 1 exhibited a very favorable logP (2.15), good aqueous solubility (logS = −1.56), low hERG liability (0.080), and moderate DILI prediction, indicating it has good pharmacokinetic potential with less risk for toxicity compared to other compounds.

Compound 7 exhibited *in vitro* (F20 = 0.360) and *in vivo* (0.809) oral bioavailability and significant BBB permeation, which suggests greater permeability of membranes and systemic absorption. Compound 25 had the highest predicted HIA (0.028) in addition to an acceptable toxicity profile, while Compound 13 had the best oral absorption probability compared to the other 11 molecules analyzed. In contrast, some compounds with high lipophilicity and poor solubility failed to achieve a higher ADMET score due to their increased probability of being toxic, as well as their reduced pharmacokinetic properties. The higher hERG's, DILI's and Ames toxicity predictions had an adverse effect on the overall ranking of several of the derivatives in Table **2**.

Overall, the ADMET investigation indicates that Compounds 1, 7, 25 and 13 have the most promising pharmacokinetic and safety profiles out of the 22 quinolinol derivatives screened and could represent viable leads for later optimization and clinical development as anti-breast cancer agents against the MCF-7 cell line.

Table 2 ADMET-Based Ranking and Drug-Likeness Properties of Quinolinol Derivatives.

S. NO.	**smiles**	**MW**	**logP**	**logS**	**caco 2**	**hia**	**f20**	**BBB**	**hERG**	**DILI**	**Ames**	**ADMET_Score**
1	Oc1cccc2ccncn12	145.05	2.154164987	-1.564415849	-4.492000615	0.01014459 1	0.23892 2656	0.12509 1702	0.08012 94	0.55095 3686	0.77110 064	6.348
7	Cc1ccc2c(O)cccc2n1	159.07	2.147190073	-2.302706344	-4.916381893	0.00179 7318	0.36038 0173	0.80914 2828	0.11672 8269	0.32233 7925	0.77796 4532	6.213
25	Nc1ccc2c(O)cccc2n1	160.06	1.266775886	-2.548052522	-4.559204609	0.02824 5091	0.19440 9311	0.51593 6255	0.08661 5808	0.57405 5731	0.91475 6119	5.768
13	O=Cc1ccc(O)c2ncccc12	173.05	1.553295755	-2.325457812	-4.770892879	0.02606 9224	0.52346 0001	0.00859 6085	0.06634 2495	0.57852 9418	0.71661 7584	5.706
19	Cc1cc(O)c2ncccc2c1	159.	2.558313376	-1.87	-4.57	0.00179	0.14601	0.09423	0.08589	0.51409	0.74044	5.492

		07		0861819	4645144	9464	7551	3811	0025	2445	2812	
17	CC(=O)c1ccc(O)c2nccccc12	187.06	1.897249618	-2.729394943	-4.605708 57	0.01307267	0.43303960 6	0.02175903 3	0.08430380 4	0.68088394 4	0.77927362 9	5.374
29	CCc1ccc(O)c2ncccc12	173.08	2.860652029	-2.572628309	-4.595503859	0.00265049 9	0.32217437	0.11440489 4	0.08492332 7	0.51699453 6	0.74156600 2	5.284
24	CCN(CC)Cc1cc(O)c2ncccc2c1	230.14	2.137904302	-1.854442974	-4.692022194	0.08154356 5	0.03599250 3	0.12941534 8	0.54590922 6	0.24411091 2	0.73003202 7	5.101
18	CN(C)Cc1ccc2c(O)cccc2n1	202.111	2.014860322	-1.874083 24	-4.901673 56	0.01908862 6	0.03346651 8	0.44600075 5	0.30983668 6	0.20126371 1	0.73286527 4	5.062
6	Oc1ccc(F)c2cccnc12	163.04	2.387328049	-2.370342435	-4.523267649	0.00118672 8	0.08837044 2	0.02626813 9	0.12563693 5	0.70824658 9	0.84648126 4	4.758
12	N#Cc1ccc(O)c2ncccc12	170.05	1.715226946	-2.224745753	-4.777646847	0.00470691 9	0.26828 14	0.00184721 1	0.20176795 1	0.63612318	0.74022221 6	4.704
8	Nc1ccc(O)c2ncccc12	160.06	-0.054424871	-1.775675982	-4.482133 44	0.00232702 5	0.03361827 1	0.33549588 9	0.06989884 4	0.76280748 8	0.91383808 9	4.486
4	[O]Nc1ccc(O)c2ncccc12	175.	1.204175338	-2.01	-4.54	0.00371	0.20561	0.03322	0.16415	0.91430	0.87329	4.385

		05		8246353	1237477	3131	6593	8081	4172	3362	2565	
28	CNc1ccc(O)c2ncccc12	174.08	1.283191376	-2.055645 87	-4.870720907	0.00378221 3	0.34084874 4	0.13855420 1	0.11403523 4	0.82950168 8	0.83998596 7	4.328
11	Oc1c(-c2ccccc2)cccc1-c1cccnc1	247.1	3.344433673	-3.045867 53	-4.697884739	0.00191015	0.00819224 1	0.58869 04	0.28028747 4	0.57206600 9	0.29967796 8	4.184
22	Oc1c(F)cc(F)c2cccnc12	181.03	2.18218325 3	-2.675025 877	-4.767838649	0.00324040 7	0.00727295 9	0.00992309 1	0.10968682 9	0.87672615 1	0.81492012 7	3.715
27	[O]Nc1cc(O)c2ncccc2c1	175.05	1.660243694	-2.260765618	-4.886774 42	0.00836491 6	0.05569827 6	0.01633880 1	0.14311154 2	0.82393503 2	0.84733259 7	3.695
2	Oc1ccc(Cl)c2cccnc12	179.01	2.993446621	-4.257819465	-4.681769747	0.00034081 9	0.04946386 8	0.05193491 3	0.09390685	0.70732522	0.72195577 6	3.498
10	Oc1ccc(CN2CCOCC2)c2cccnc12	244.12	1.287293281	-2.332085116	-4.819310306	0.00190335 5	0.05741548 5	0.01815230 4	0.24850623 3	0.53782635 9	0.72635895	3.294
21	Cc1ccc(-c2ccc(O)c3ncccc23)cc1	235.1	3.813838235	-3.669364894	-4.496861 56	0.00054162 7	0.15150833 1	0.14299893 4	0.23814711	0.74625319 2	0.76063406 5	3.101
9	Oc1ccc(CN2CCCCC2)c2cccnc12	242.14	2.709077639	-2.650599423	-4.861772526	0.00036907 2	0.01849 86	0.09429892 9	0.60819721 2	0.29763904 2	0.54170012 5	3.082

3	Oc1c(Cl)cc(Cl)c2cccnc12	212.97	3.190513 83	-4.433004476	-4.922881 13	0.00039 1662	0.00163 43	0.00933 3431	0.13938 4031	0.82778 7578	0.58598 9118	2.286

3.4 Molecular docking

The molecular docking study was conducted on selected quinolinol derivatives to assess the binding affinity and interaction profiles within the active binding site of the human estrogen receptor alpha (ER-alpha) protein (PDB ID: 3ERT) which is a well-characterized therapeutic target for breast cancer. The results of the docking analysis indicated that each of the screened quinolinol derivatives had greater binding affinities for the ER-alpha than the standard reference drug tamoxifen, suggesting that these compounds may have potential as anticancer agents in the MCF7 breast cancer cell line (Refer to Fig **6**). Of the quinolinol derivatives screened, ligand 7 had the greatest docking score of -11.98 kcal/mol, with ligand 1 having a docking score of -11.48 kcal/mol, ligand 25 having a docking score of -11.04 kcal/mol and ligand 13 having a docking score of -9.46 kcal/mol; these values are all higher than the reference compound 4-hydroxytamoxifen which had a docking score of -8.26 kcal/mol as shown in Table **3**.

Table 3 Molecular Docking Scores and Binding Interactions of Selected Quinolinol Derivatives Against ER-α (PDB ID: 3ERT).

Ligands	**Docking Score (kcal/mol)**	**Amino Acid Residues Involved**	**Interactions**
Ligand 7	−11.98	Leu346, Leu349, Glu353, Gly390, Met357, Leu525, Phe404	Hydrogen bonding, Hydrophobic interactions, π–π stacking
Ligand 1	−11.48	Ala350, Glu353, Arg394, Gly390, Leu525, Met357	Hydrogen bonding, Hydrophobic interactions

Ligand 25	−11.04	Leu346, Glu353, Gly390, Arg394, Met357	Hydrogen bonding, Electrostatic and Hydrophobic interactions
Ligand 13	−9.46	Leu349, Ala350, Glu353, Gly390, Leu525	Hydrophobic interactions, Hydrogen bonding
4-Hydroxytamoxifen	−8.26	Leu346, Leu349, Ala350, Glu353, Arg394, Gly390	Hydrogen bonding, Hydrophobic interactions, π–π stacking

Based on the analysis of docking energies, the selected ligands exhibited greater strength and stability of binding to the ER-α active site than did the standard therapeutic agent. All four quinolinol derivatives occupied the same active pocket as 4-hydroxytamoxifen in the receptor and interacted with the same amino acid residues important for stabilizing the ligand in the receptor cavity. Additionally, the hydrophobic interactions, hydrogen bonds, and π–π stacking interactions of our selected quinolinol derivatives and 4-hydroxytamoxifen occurred with the following residues: Leu346, Leu349, Ala350, Glu353, Arg394, Gly390, Leu525, Met357, and Phe404. The presence of these shared residues in both the selected quinolinol derivatives and 4-hydroxytamoxifen provides strong support for the selected quinolinol derivatives mimicking the binding orientation of 4-hydroxytamoxifen within the ER-α receptor binding domain. Ligand 7 established highly stable binding interactions based upon hydrogen bonding with key active-site residues and also established numerous hydrophobic contacts within the receptor cavity, resulting in a superior docking score. Ligands 1 and 25 also formed significant hydrophobic and hydrogen bond interactions with the conserved amino acids lining the active pocket. Ligand 13 stabilized its binding by forming favorable electrostatic and hydrophobic interactions, but its overall docking affinity was slightly lower than that of the highest-ranked ligands.

The results of the 3D docking studies supported the labeling of the quinolinol derivatives as tightly packed into the hydrophobic binding site of ER-α with networks of interactions similar to that of the co-crystallized ligand 4-hydroxytamoxifen. The identical binding orientations and amino acids profiles suggest that these compounds may inhibit the ER-α signaling pathways

involved in MCF-7 breast cancer cell growth. Based on the docking studies, the quinolinol derivatives, including Ligands 7, 1, and 25, have a high probability of binding well to ER-α and will therefore serve as useful lead compounds for further anti-breast cancer drug discovery.

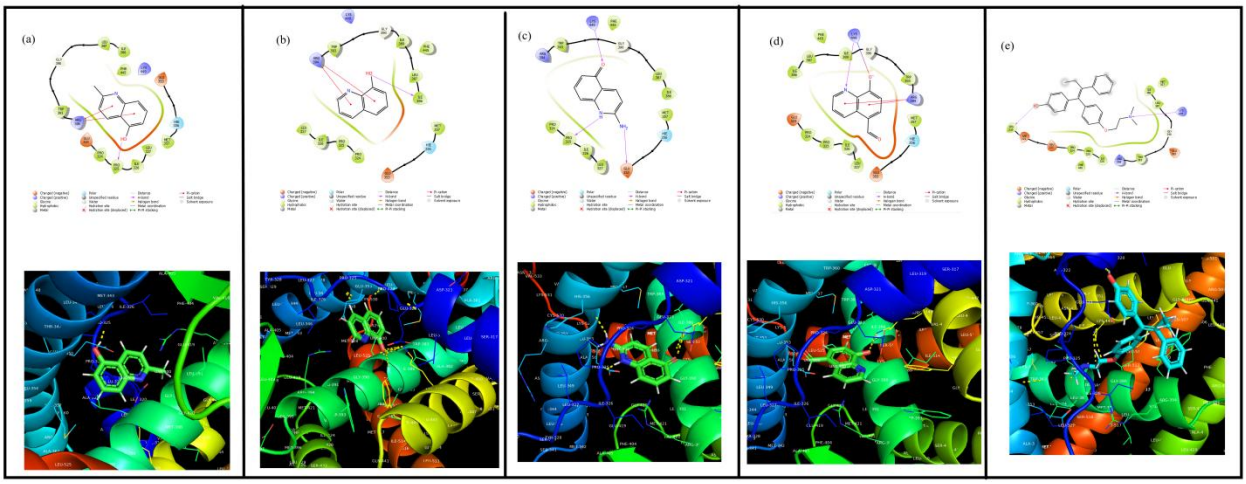


Fig.6. 2D and 3D visualization of molecular docking interaction analysis of selected quinolinol derivatives and 4-hydroxytamoxifen within the active site of ER-α (pdb id: 3ert).

3.5 Molecular dynamic simulation

The molecular dynamics (MD) study was conducted over 100 nanoseconds to determine the dynamic behaviour and structural stability (Fig **7**) of ligand 7 (an isomer with two aromatic groups) with the receptor protein ER-α (PDB: 3ERT). For 4-hydroxytamoxifen (also known as 4-OHT), a standard drug, the analysis of root mean square deviation (RMSD), radius of gyration (Rg), root mean square fluctuation (RMSF), and ligand-RMSF profiles were compared, and it was determined that ligand 7 forms a more stable and compact complex to the receptor protein than 4-OHT over the duration of the simulation (Fig **7**). When observing Fig **7**A, the RMSD trajectory of each of the protein-ligand complexes is overlaid from the 100 nanoseconds of simulation; both complexes increase slightly during the first 10 nanoseconds (during equilibration), and the complexation of ligand 7 reached greater stabilization rapidly after approximately 15 nanoseconds, resulting in an RMSD range of 0.24 to 0.28 nm for the remainder of the 100 nanoseconds of the simulation, while the complexation of 4-OHT had a relatively higher fluctuation of RMSD between 20-60 nanoseconds and 70-100 nanoseconds, indicating that 4-OHT has lower structural stability than ligand 7. When compared to 4-OHT, the average RMSD of ligand 7 was lower and showed less fluctuation, therefore indicating a stronger stabilization effect of ligand 7 in the active pocket of the ER-α receptor protein. Figure 7B shows how tightly packed the proteins were throughout the simulations by plotting their radius of gyration (Rg). The two complexes had fairly consistent values for Rg (around 2.30-2.34 nm for both), so there was no detectable unfolding of the receptor proteins. On the other hand, the fluctuations in Rg of the Ligand 7 complex were much less varied over the entire course of the 100 ns simulation (especially from 20 ns to 80 ns), indicating that Ligand 7 was more compact and conformationally stable than the 4-OHT complex.

In the RMSF study reported in Fig. **7**C, analysis of the amino acids making up the ER-α ligand binding cavity was conducted over the course of the simulation, with the residues interacting with Ligand 7 exhibiting the most stable interactions (i.e., low fluctuation values of < 0.20 nm) at the active site. The few loop regions characterized by fluctuation values of moderate magnitude (80–100, 250–280 and 450–500 amino acid residues) in the ER-α protein indicated that these were the most flexible regions in the ER-α and Ligand 7 complex relative to its flexibility compared to 4-OHT. The active site residues involved in ligand binding to the ER-α exhibited little fluctuation, thus confirming the existence of stable intermolecular interactions over the duration and throughout the simulation. The RMSF plot for the ligand, Fig. **7**D, supports the conclusion that Ligand 7 is more stable than 4-OHT based on the greater fluctuations observed for several of 4-OHT's terminal atoms compared to the other terminal atoms associated with Ligand 7 during the simulation period. The 4-OHT demonstrated significant fluctuations beginning after the first 40 atoms of the trajectory, while the majority of the atoms of Ligand 7 remained relatively stable over the duration of the trajectory. Therefore, Ligand 7 demonstrates a greater degree of rigidity and stability in the ER-α binding pocket than does the reference drug 4-hydroxytamoxifen, as shown in the MD simulation study (PDB ID: 3ERT). A lower root-mean-square deviation and root-mean-square fluctuation together with the stability of the radius of gyration during the 100 ns simulation period indicates that Ligand 7 had better conformational stability, was more compact, and had higher binding persistence over this time period. This indicates that Ligand 7 could potentially be an effective therapeutic candidate against breast cancer when targeting the MCF-7 cell line..

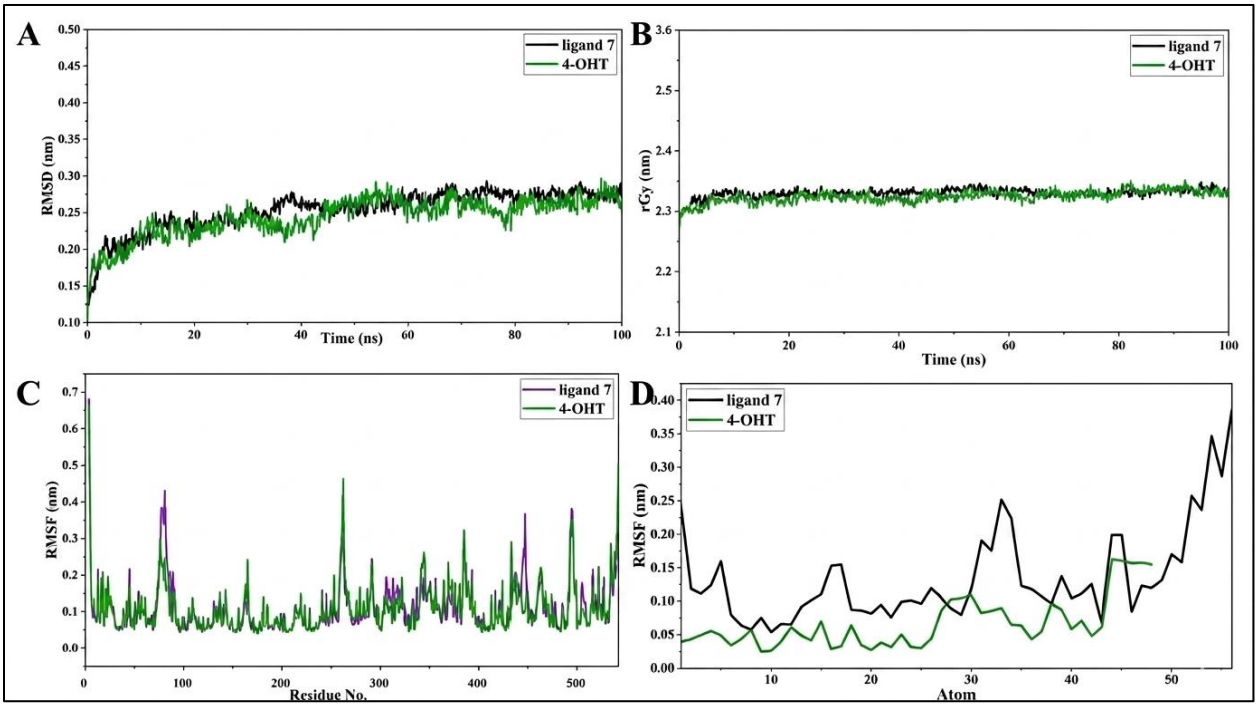


Fig. 7. **A** RMSD, **B** Radius of Gyration during 100 ns MD Simulation. and **C, D** RMSF Profiles of ER-α Complexes with Ligand 7 and 4-Hydroxytamoxifen.

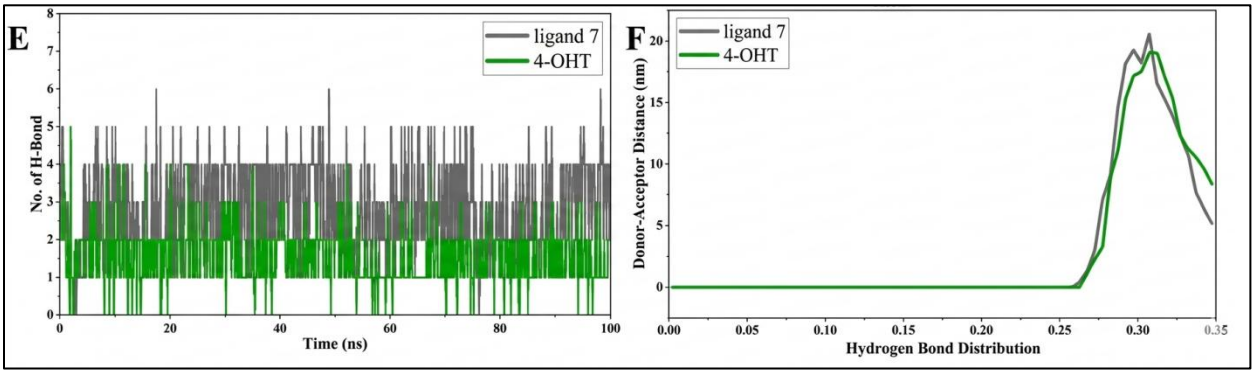


Fig. 7 E Dynamic Hydrogen Bond Interaction. **F** Hydrogen Bond distribution of Ligand 7 and Standard Drug 4-OHT Against ER-α (3ERT)

During a 100 ns molecular dynamics simulation of the hydrogen bonding analysis there were additional confirmations of the binding stability of Ligand 7 versus its referential structure, 4-hydroxytamoxifen (4-OHT), at the active site of ER-α (PDB ID: 3ERT) (Fig. **7**).

Fig. **7**E represents a visual interpretation of the number of hydrogen bonds established between our ligands and receptor protein throughout the entire simulation trajectory. 4-OHT maintained its number of hydrogen bonds during an approximate period of 100ns; however, Ligand 7 consistently sustained its number of hydrogen bonds greater than that of Ligand 4-OHT over the entire simulation period. The Ligand 7 complex maintained, on average, 2–5 stable hydrogen bonds (with occasional peaks of 6 to 8 in number) during the intervals between 10–25 ns, 40–60 ns, and 70–100 ns throughout the simulation. While, 4-OHT was primarily established with only 1–3 hydrogen bonds and had a greater number of variable coefficients compared to its average number of hydrogen bonds. The persistence of greater hydrogen bonding for Ligand 7 indicated a higher degree of intermolecular interactions and increased stability of the ligand within the ER-α binding pocket. Fig **7**F represents the distribution of hydrogen bond distances established between donor and acceptor atoms in both complexes. Ligand 7 demonstrated a distinct and consistent peak in the distribution of hydrogen bond distances around 0.29–0.31 nm, which is within the defined range for optimal hydrogen bonding distance, demonstrating an increased degree of stable and strong donor–acceptor interactions throughout the entire simulation. While both 4-OHT and ligand 7 had similar distances of hydrogen bonding, 4-OHT had a larger distribution and lower peak height showing that these hydrogen bonds were weaker and not as stable compared to ligand 7. The total number of hydrogen bonds formed between ligand 7 and the active site residues of ER-α was greater for ligand 7, indicating that ligand 7 forms stronger and more stable hydrogen bonds with ER-α compared to those of the therapeutic drug 4-OHT. These data, collectively, support a significantly higher binding affinity, greater complex stability, and greater inhibitory effect of ligand 7 against the target protein MCF-7 breast cancer.

3.6 Density Functional Theory

The electronic properties of Ligand 7 and 4-Hydroxytamoxifen were analyzed using Density Functional Theory (DFT), the results of which are summarized in Table **4**. Ligand 7's (shown as Fig. **8**A - C) highest occupied molecular orbital (HOMO) energy was found to be −5.6776 eV and its lowest unoccupied molecular orbital (LUMO) energy was found to be −1.4657 eV, giving Ligand 7 a total energy gap of 4.2119 eV. Conversely, 4-Hydroxytamoxifen (shown as Fig. **8**D - F) has a HOMO energy of −4.6571 eV and a LUMO of −1.8019 eV with a total energy gap of only 2.8552 eV. Because of this lower energy gap, 4-Hydroxytamoxifen has a higher degree of chemical reactivity, lower kinetic stability and provides for a greater degree of electron transfer compared to Ligand 7. Ligand 7 has a higher number of electrons in its structure, meaning that it possesses more kinetic stability and a lower degree of chemical softness than 4-Hydroxytamoxifen.

The molecular electrostatic potential (MEP) maps generated from this investigation of the two compounds indicate that the presence of oxygen-containing functional groups of Ligand 7 and 4-Hydroxytamoxifen (specifically hydroxyl (-OH), carbonyl (C=O), and ethers) are highly likely to serve as the electron-rich regions where electrophilic attack occurs and hydrogen bonding occurs, while the aromatic rings and hydrophobic alkyl chains in the chemical structures of Ligand 7 and 4-Hydroxytamoxifen would promote hydrophobic interactions in the receptor cavity. In conjunction with the initial analyses of the compounds, additional docking studies confirmed that Ligand 7 has significantly better docking scores over 4-Hydroxytamoxifen (−11.98 and −8.26 kcal/mol), suggesting that it interacts with the target protein than does 4-Hydroxytamoxifen. Several amino acid residues within the pocket of the protein form hydrogen bonds, hydrophobic interactions, and π-π stacking with Ligand 7, including Leu346, Leu349, Glu353, Gly390, Met357, Leu525, and Phe404. A similar mode of interaction exists between 4-Hydroxytamoxifen and a number of these same amino acid residues, including Leu346, Leu349, Ala350, Glu353, Arg394, and Gly390. Therefore, due to the favourable electronic distribution and optimal alignment of the frontier molecular orbitals, in addition to the multiple functional groups present that can potentially form such interactions, Ligand 7 demonstrates a greater potential than 4-Hydroxytamoxifen as a bioactive compound.

Table 4. Calculated DFT Parameters of Ligand 7 and 4-Hydroxytamoxifen

DFT Parameter	**Ligand 7**	**4-Hydroxytamoxifen**
HOMO Energy (eV)	−5.6776	−4.6571
LUMO Energy (eV)	−1.4657	−1.8019
Energy Gap, (E_g) (eV)	4.2119	2.8552

Ionization Potential, (I) (eV)	5.6776	4.6571
Electron Affinity, (A) (eV)	1.4657	1.8019
Chemical Hardness, (eta) (eV)	2.1059	1.4276
Chemical Softness, (S) (eV^{-1})	0.2374	0.3502
Chemical Potential, (mu) (eV)	−3.5717	−3.2295
Electronegativity, (chi) (eV)	3.5717	3.2295
Electrophilicity Index, (omega) (eV)	3.0291	3.6518
Stability	Higher	Moderate
Reactivity	Lower	Higher

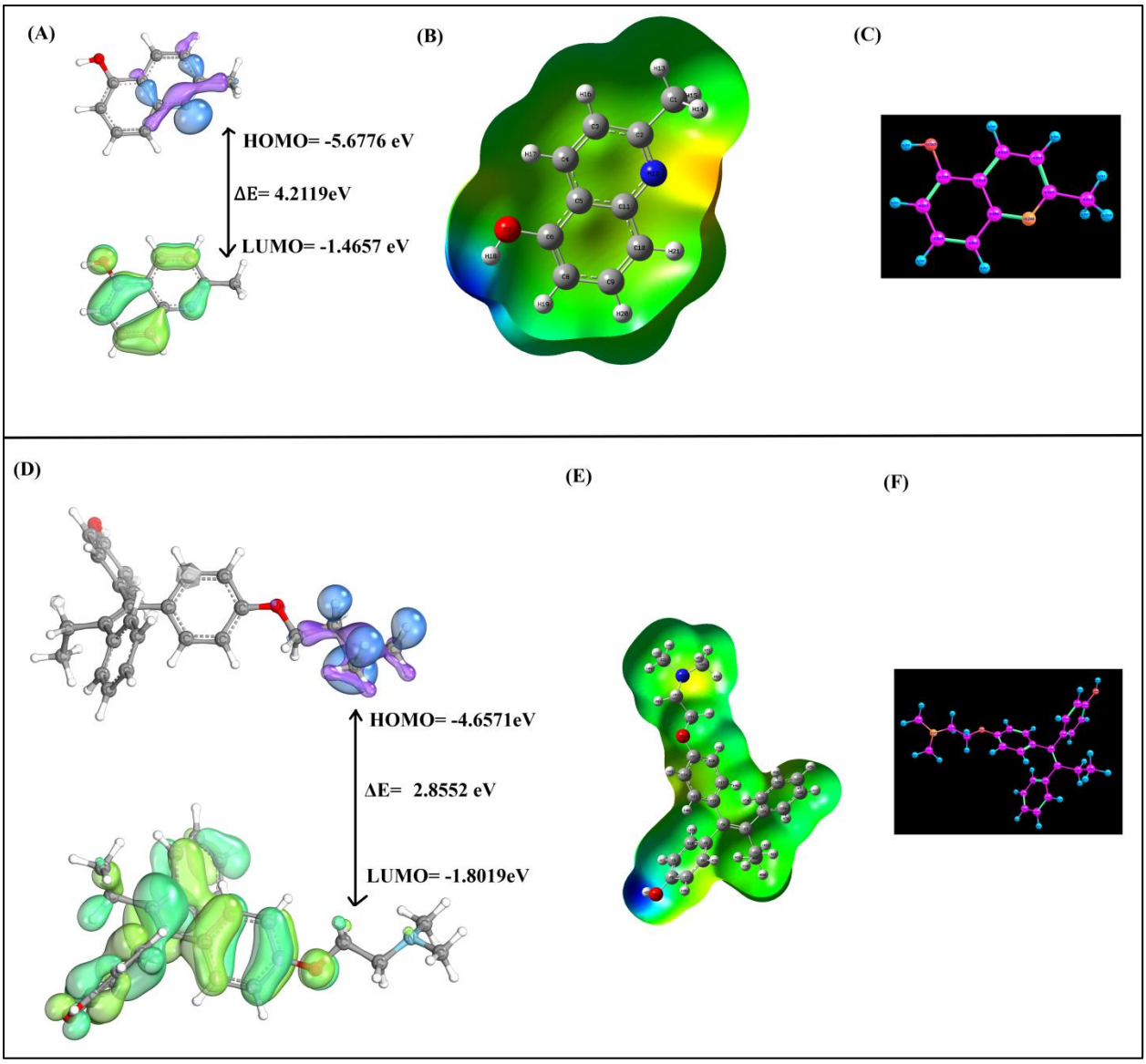


Fig. 8 A,D Frontier molecular orbital distributions showing the HOMO and LUMO energy levels of the ligand 7 and 4-OHT respectively along with the calculated energy gaps (ΔE). **B,E** Molecular electrostatic potential (MEP) surfaces of ligand 7 and 4-OHT respectively showing the electron-rich and electron-deficient regions over the molecular framework. **C** mulliken charges distribution over the atoms in ligand 7. **F** mulliken charges distribution over the atoms in 4-OHT.

4 Development of lead formula

Quinolinol derivatives of the structural determinants and the topographic binding modes of the quinolinol derivatives in the ER-α ligand-binding region (Fig. **9**). The localized structure shows that the heterocyclic quinolinol core is a very rigid anchor for the compound within the active site pocket; it forms a strong pi-pi-stacking network with ARG394 at their fused aromatic rings. The endocyclic N atom of the quinolinol also makes a H-bond with PRO325 that stabilizes the core of the compounds. Electrostatic complementarities and the binding free energy of the scaffolds were

significantly affected by the systematic peripheral modifications to the quinolinol ring system, especially at the R1 position (hydroxyl, carbonyl or acyl) and the R2 position (hydroxyl or oxididyl) as hydrophilic- functionalized groups at these positions created hydrogen bonding networks with PRO325, LYS449 and ILE386 and thus drove binding affinities for each of the groups. In addition to peripheral modifications, structural and spatial modifications made at the R3 position by using very compact methyl or amine substitutions leveraged localized hydrophobic characteristics to achieve maximum geometric fit and complementarity to those created by the shapes of the compound inside the ligand-binding domain of the estrogen receptor α and were accomplished without creating steric hindrance.

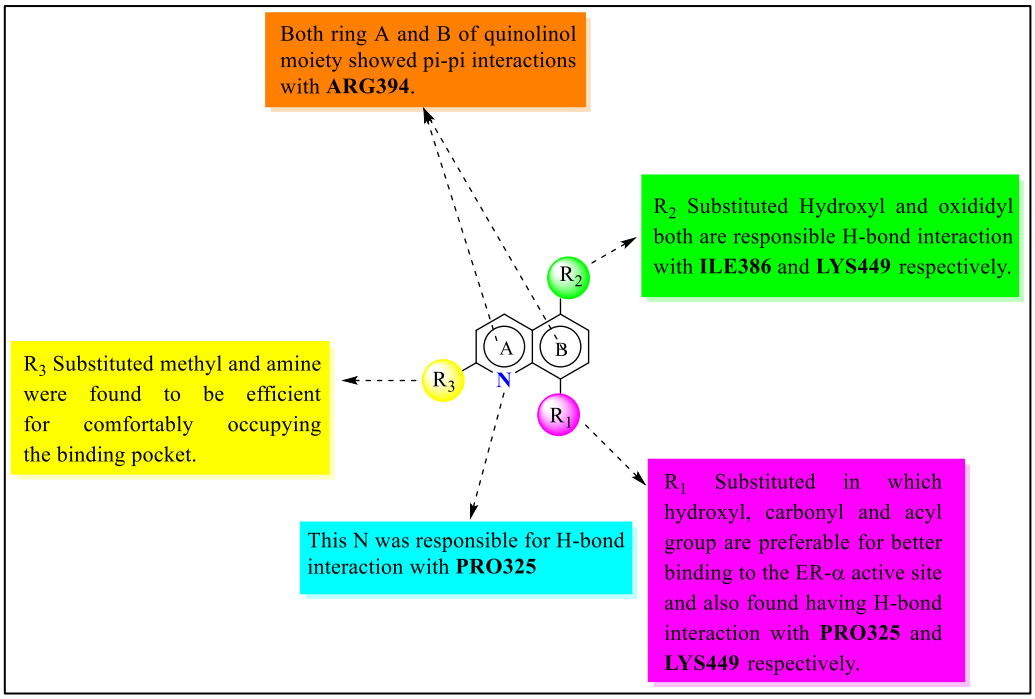


Fig. 9 structural requirements R_1, R_2, R3 and crucial amino acid interactions of the quinolinol moiety for optimal binding affinity at the ER-α active site.

5 Conclusion

In this research, a comprehensive computational pipeline consisting of 3D-QSAR and pharmacophore modeling, virtual screening, molecular docking, ADMET prediction, molecular dynamics (MD) simulations, and DFT evaluation was established in the search for effective quinolinol compounds to target the estrogen receptor alpha (ER-α) for breast cancer treatment in the MCF-7 cell line. The use of a Gaussian field-3D-QSAR predictive model provided insight into the steric, electrostatic, and hydrogen-bonding requirements for increased inhibition. The three-dimensional characterization of these compounds, along with the successful development of a robust pharmacophore model from the structure-activity relationship (SAR), enabled the use of these three-dimensional spectroscopic models to perform hierarchical virtual screening of approximately 400,000 PubChem compounds. The results of molecular docking studies suggest

that the quinolinol compounds exhibiting the top four hits bind significantly more strongly to ER-α than the standard therapeutic, 4-hydroxytamoxifen, which returned a docking score of (−11.98 kcal/mol) for Ligand 7, with significant preliminary scores for Ligands 1, 25, and 13. Additionally, results from predictive ADMET and DFT assessments suggest that these top quinolinol candidates are predicted to exhibit favourable biological and pharmacological properties. Furthermore, Ligand 7 was shown to produce a highly compact and stable complex with ER-α in the context of 100 ns MD simulation, which was shown to maintain better conformational stability and hydrogen-bonding persistence than the standard therapeutic. Ligand 7 is a strong candidate for the development of new therapies to treat breast cancer, and *in vitro* and *in vivo* experimental validations are required.

Acknowledgements
The authors gratefully acknowledge Guru Ghasidas Vishwavidyalaya (GGU), Bilaspur, India, for providing the institutional support, laboratory facilities, and computational resources for this study.

Author Contributions
Mayank Garhewal: writing-original draft preparation, conceptualization, methodology, writing-reviewing and editing.
Divya Pujari, Avantika agrawal, Dr. Achal Mishra, Dr. Yogesh Vaishnav, Aditya mishra, Dr. Shekhar Verma, Ayush Tiwari, Dr. Arin Bhattacharya: data curation, visualization, validation, Formal analysis, Investigation.

Funding
The authors received no financial support for this research.

Data availability
In silico data and material are present in the manuscript.

Declarations

Ethics approval and consent to participate
Not applicable. This study did not involve human participants or animals, and ethical approval was not required.

Consent for publication
Not applicable.

Competing interests
The authors declare no competing interests.

REFERENCES

1. Sung H, Ferlay J, Siegel RL, Laversanne M, Soerjomataram I, Jemal A, Bray F. Global cancer statistics 2020: GLOBOCAN estimates of incidence and mortality worldwide for 36 cancers in 185 countries. *CA: A Cancer Journal for Clinicians*. 2021 May;71(3):209-49.
2. Lumachi F, Santeufemia DA, Basso SM. Current medical treatment of estrogen receptor-positive breast cancer. *World Journal of Biological Chemistry*. 2015 Aug 26;6(3):231-39.
3. Yaşar P, Ayaz G, User SD, Güpür G, Muyan M. Molecular mechanism of estrogen-estrogen receptor signaling. *Reproductive Medicine and Biology*. 2017 Jan;16(1):4-20.
4. Shagufta, Ahmad I. Tamoxifen a pioneering drug: An update on the therapeutic potential of tamoxifen derivatives. *European Journal of Medicinal Chemistry*. 2018 Jan 1;143:515-31.
5. Chang M. Tamoxifen resistance in breast cancer. *Biomolecules & Therapeutics*. 2012 May;20(3):256-67.
6. Kerru N, Gummidi L, Maddila S, Gangu KK, Jonnalagadda SB. A review on recent advances in nitrogen-containing molecules and their biological applications. *Molecules*. 2020 May;25(8):1909.
7. Matada BS, Pattanashetty R, Yernale NG, Kalkhambkar RG. A comprehensive review on the biological interest of quinoline and its derivatives. *Bioorganic & Medicinal Chemistry*. 2021 Mar 1;32:115973.
8. Sliwoski G, Kothiwale S, Meiler J, Lowe EW. Computational methods in drug discovery. *Pharmacological Reviews*. 2014 Jan;66(1):334-95.
9. Verma J, Khedkar VM, Coutinho EC. 3D-QSAR in drug design—a review. *Current Topics in Medicinal Chemistry*. 2010 Jan 1;10(1):95-115.
10. Meng XY, Zhang HX, Mezei M, Cui M. Molecular docking: a powerful approach for structure-based drug discovery. *Current Computer-Aided Drug Design*. 2011 Jun;7(2):146-57.
11. Guan L, Yang H, Cai Y, Sun L, Di P, Li W, Liu G, Tang Y. ADMET-score–a comprehensive scoring function for evaluation of chemical drug-likeness. *MedChemComm*. 2019;10(1):148-57.
12. Hollingsworth SA, Dror RO. Molecular dynamics simulation for all. *Neuron*. 2018 Sep 19;99(6):1129-43.
13. Muralikrishnan AM, Kubavat JA, Vasava MA, Jupudi SR, Biju NA. Investigation of anti-sars cov-2 activity of some tetrahydro curcumin derivatives: an in silico study. Int J App Pharm. 2023;15(1):333-9.
14. Yusuf AJ, Adegboyega AE, Yakubu AH, Johnson GI, Asomadu RO, Adeduro MN, Chukwuma IF, Ugwah-Oguejiofor CJ, Okoh OS, Johnson TO. Exploring Scutellaria baicalensis bioactives as EGFR tyrosine kinase inhibitors: cheminformatics and molecular docking studies. Informatics in Medicine Unlocked. 2023 Jan 1;43:101406.
15. Kulkarni S, Singh Y, Biharee A, Bhatia N, Monga V, Thareja S. Molecular docking, 3D-QSAR and simulation studies for identifying pharmacophoric features of indole derivatives

as 17β-hydroxysteroid dehydrogenase type 5 (17β-HSD5) inhibitors. Journal of Biomolecular Structure and Dynamics. 2023 Dec 29;41(22):12668-85.
16. Mohamed LM, Eltigani MM, Abdallah MH, Ghaboosh H, Bin Jardan YA, Yusuf O, Elsaman T, Mohamed MA, Alzain AA. Discovery of novel natural products as dual MNK/PIM inhibitors for acute myeloid leukemia treatment: pharmacophore modeling, molecular docking, and molecular dynamics studies. Frontiers in Chemistry. 2022 Jul 22;10:975191.
17. Li X, Li L, Zhang N, Wang L, Luo L. Structure-Based Virtual Screening for ALOX5 Inhibitors: Combining Scaffold Hopping and Pharmacophore Approaches. Targets. 2026 Feb 12;4(1):8.
18. Ibraheem W, Alsheikh F, Alzain AA, Bhongade BA, Ejaz L, Baig H, Robinson RC, El-Tanani M. Computational repurposing of approved drugs targeting KRAS G12D and EGFR for colorectal cancer therapy. PLoS One. 2026 Jan 28;21(1):e0338123.
19. Yao, S.; Fan, L. Y.; Lam, E. W., The FOXO3-FOXM1 axis: A key cancer drug target and a modulator of cancer drug resistance. Semin. Cancer. Biol., 2018, 50, 77-89. DOI: 10.1016/j.semcancer.2017.11.018, PMID 29180117.